

INFRARED PHOTOMETRY OF LATE-M, L, AND T DWARFS

S. K. LEGGETT,¹ DAVID A. GOLIMOWSKI,² XIAOHUI FAN,³ T. R. GEBALLE,⁴ G. R. KNAPP,⁵ J. BRINKMANN,⁶
ISTVÁN CSABAI,^{2,7} JAMES E. GUNN,⁵ SUZANNE L. HAWLEY,⁸ TODD J. HENRY,^{2,9} ROBERT HINDSLEY,¹⁰
ŽELJKO IVEZIĆ,⁵ ROBERT H. LUPTON,⁵ JEFFREY R. PIER,¹¹ DONALD P. SCHNEIDER,¹² J. ALLYN SMITH,¹³
MICHAEL A. STRAUSS,⁵ ALAN UOMOTO,² AND D. G. YORK¹⁴

Received 2001 May 28; accepted 2001 August 27

ABSTRACT

We present *ZJHKLM'* photometry of a sample of 58 late M, L, and T dwarfs, most of which are identified from the Sloan Digital Sky Survey and the Two Micron All-Sky Survey. Near-infrared spectra and spectral classifications for most of this sample are presented in a companion paper by Geballe et al. We derive the luminosities of 18 dwarfs in the sample with known parallaxes, and the results imply that the effective temperature range for the L dwarfs in our sample is approximately 2200–1300 K and for the T dwarfs 1300–800 K. We obtained new photometric data at the United Kingdom Infrared Telescope for: 42 dwarfs at *Z*, 34 dwarfs at *JHK*, 21 dwarfs at *L'*, as well as *M'* data for two L dwarfs and two T dwarfs. The *M'* data provide the first accurate photometry for L and T dwarfs in this bandpass—for a T2 and a T5 dwarf, we find $K - M' = 1.2$ and 1.6, respectively. These colors are much bluer than predicted by published models, suggesting that CO may be more abundant in these objects than expected, as has been found for the T6 dwarf Gl 229B. We also find that $K - L'$ increases monotonically through most of the M, L, and T subclasses, but it is approximately constant between types L6 and T5, restricting its usefulness as a temperature indicator. The degeneracy is probably due to the onset of CH₄ absorption at the blue edge of the *L'* bandpass. The *JHK* colors of L dwarfs show significant scatter, suggesting that the fluxes in these bandpasses are sensitive to variations in photospheric dust properties. The *H - K* colors of the later T dwarfs also show some scatter, which we suggest is due to variations in pressure-induced H₂ opacity, which is sensitive to gravity and metallicity.

Subject headings: infrared: stars — stars: fundamental parameters — stars: late-type — stars: low-mass, brown dwarfs

1. INTRODUCTION

For most of the twentieth century, the classical Harvard spectral types—OBAFGKM—spanned the temperature range of all known main-sequence dwarfs. The discoveries of very cool companions to the white dwarf GD 165 (Becklin & Zuckerman 1988) and the M dwarf Gliese 229 (Nakajima et al. 1995), however, foreshadowed the first

extension of the Harvard system in nearly 100 yr. GD 165B is now known to have $T_{\text{eff}} \approx 1900$ K and a probable mass of $\sim 0.07 M_{\odot}$, placing it near the stellar-substellar mass boundary (Kirkpatrick et al. 1999a). With $T_{\text{eff}} \approx 950$ K and a mass of $0.015\text{--}0.07 M_{\odot}$ (Saumon et al. 2000), Gl 229B is cool enough to show methane absorption in its near-infrared spectrum and is unambiguously substellar (i.e., a brown dwarf). These two objects remained unique until the late 1990's, when new sky surveys began revealing significant numbers of similar objects in the field.

In 1997, several GD 165B-like objects were discovered from two near-infrared sky surveys, the Two Micron All-Sky Survey (2MASS; Kirkpatrick, Beichman, & Skrutskie 1997) and the DEEP Near-Infrared Survey (DENIS; Delfosse et al. 1997), as well as a southern hemisphere proper motion survey (Ruiz, Leggett, & Allard 1997). In 1999 several Gl 229B-like brown dwarfs were found in the commissioning data of the Sloan Digital Sky Survey (SDSS; Strauss et al. 1999; Tsvetanov et al. 2000), the 2MASS database (Burgasser et al. 1999), and the New Technology Telescope Deep Field (Cuby et al. 1999). GD 165B and Gl 229B became the respective prototypes of two new spectral classes, L and T (Kirkpatrick et al. 1999b; Martín et al. 1999b). Over 100 L dwarfs and tens of T dwarfs are now known.

In this paper, we present $0.95\text{--}4.70 \mu\text{m}$ photometry of 58 late-M, L, and T dwarfs obtained with the United Kingdom Infrared Telescope (UKIRT). We describe the sample in § 2 and present the photometry in § 3. In § 4 we derive the luminosity and estimate the temperature of 18 M, L, and T dwarfs for which parallaxes are known, to place our sample in a physical context. In § 5 we discuss the correlation of the

¹ United Kingdom Infrared Telescope, Joint Astronomy Centre, 660 North A'ohoku Place, Hilo, HI 96720; skl@jach.hawaii.edu.

² Department of Physics and Astronomy, The Johns Hopkins University, 3400 North Charles Street, Baltimore, MD 21218; dag@pha.jhu.edu.

³ Institute for Advanced Study, Einstein Drive, Princeton, NJ 08540; fan@ias.edu.

⁴ Gemini Observatory, 670 North A'ohoku Place, Hilo, HI 96720; tgeballe@gemini.edu.

⁵ Princeton University Observatory, Princeton, NJ 08544; gk@astro.Princeton.edu.

⁶ Apache Point Observatory, 2001 Apache Point Road, P.O. Box 59, Sunspot, NM 88349.

⁷ Department of Physics and Complex Systems, Eötvös University, Pázmány Péter sétány 1/A, Budapest, H-1117, Hungary.

⁸ Department of Astronomy, University of Washington, Box 351580, Seattle, WA 98195.

⁹ Department of Physics and Astronomy, Georgia State University, Atlanta, GA 30303.

¹⁰ Remote Sensing Division, United States Naval Research Laboratory, Washington, DC 20375.

¹¹ US Naval Observatory, Flagstaff Station, P.O. Box 1149, Flagstaff, AZ 86002-1149.

¹² Department of Astronomy and Astrophysics, The Pennsylvania State University, University Park, PA 16802.

¹³ Department of Physics and Astronomy, University of Wyoming, P.O. Box 3905, Laramie, WY 82071.

¹⁴ University of Chicago, Astronomy and Astrophysics Center, 5640 South Ellis Avenue, Chicago, IL 60637.

TABLE 1
THE SAMPLE

Name	R.A. (J2000)	Decl. (J2000)	Distance Modulus $M - m$ (error)	References ^a	Spectral Type ^b
BRI 0021-0214	00 24 24.6	-01 58 22	-0.42 (0.08)	1	M9.5
2MASS J0028+15	00 28 39.4	+15 01 41	...		L3
SDSS 0032+14	00 32 59.4	+14 10 37	...		L8
2MASSW J0036+18	00 36 15.9	+18 21 10	0.30 (0.02)	2	L4
SDSS 0107+00	01 07 52.3	+00 41 56	...		L5.5
SDSS 0151+12	01 51 41.7	+12 44 30	...		T1
LHS 11	02 00 10.0	+13 03 06	1.76 (0.03)	1	M5
DENIS-P J0205-11AB	02 05 29.0	-11 59 25	-1.13 (0.10)	3	L5.5
SDSS 0207+00	02 07 42.8	+00 00 56	...		T4.5
SDSS 0236+00	02 36 17.9	+00 48 55	...		L6.5
2MASSW J0310+16	03 10 59.9	+16 48 16	...		L9
2MASSW J0328+23	03 28 42.6	+23 02 05	...		L9.5
2MASP J0345+25	03 45 43.2	+25 40 23	-2.18 (0.04)	3	L1
SDSS 0423-04	04 23 48.6	-04 14 04	...		T0
SDSS 0539-00	05 39 52.0	-00 59 02	...		L5
2MASSW J0559-14	05 59 19.1	-14 04 48	...		T4.5
Gl 229B	06 10 34.7	-21 51 49	1.19 (0.02)	4	T6
2MASS J0746+20AB	07 46 42.5	+20 00 32	-0.44 (0.02)	2	L1
2MASS J0825+21	08 25 19.6	+21 15 52	-0.48 (0.33)	5	L6
SDSS 0830+48	08 30 08.1	+48 28 47	...		L9
SDSS 0837-00	08 37 17.2	-00 00 18	...		T0.5
2MASSs J0850+10AB	08 50 35.9	+10 57 16	-2.47 (0.34)	3	L6 ^c
SDSS 0857+57	08 57 58.5	+57 08 51	...		L8
SDSS 0926+58	09 26 15.4	+58 47 21	...		T4.5
2MASSW J0929+34	09 29 33.6	+34 29 52	...		L8 ^c
SDSS 1021-03	10 21 09.7	-03 04 20	...		T3
2MASS J1047+21	10 47 53.9	+21 24 23	...		T6.5
LHS 292	10 48 13.0	-11 20 12	1.72 (0.04)	1	M6.5
LHS 36	10 56 28.9	+07 00 52	3.11 (0.01)	1	M6
DENIS-P J1058-15	10 58 46.5	-15 48 00	-1.22 (0.04)	3	L3
LHS 2347	11 05 09.0	+07 06 48	...		M5
SDSS 1110+01	11 10 10.0	+01 16 13	...		T6
LHS 2397a	11 21 49.0	-13 13 08	-0.77 (0.07)	1	M8
LHS 315	11 47 45.0	+00 48 24	2.38 (0.02)	4	M4
2MASSW J1217-03	12 17 11.1	-03 11 13	...		T8
2MASSW J1225-27	12 25 54.3	-27 39 47	...		T6
DENIS-P J1228-15AB	12 28 13.8	-15 47 11	-1.29 (0.11)	3	L6
LHS 333AB	12 33 17.0	+09 01 18	1.79 (0.04)	1	M4
SDSS 1254-01	12 54 53.9	-01 22 47	...		T2
SDSS 1257-01	12 57 37.3	-01 13 36	...		L5
Kelu-1	13 05 40.2	-25 41 06	-1.40 (0.08)	3	L3
SDSS 1314-00	13 14 15.5	-00 08 48	...		L2
SDSS 1326-00	13 26 29.8	-00 38 32	...		L5.5
SDSS 1346-00	13 46 46.5	-00 31 50	...		T6
GD 165B	14 24 39.9	+09 17 16	-2.49 (0.17)	1	L3
LHS 2924	14 28 43.4	+33 10 42	-0.17 (0.03)	1	M9
2MASSW J1439+19	14 39 28.4	+19 29 15	-0.78 (0.02)	3	L1 ^c
SDSS 1446+00	14 46 00.6	+00 24 52	...		L5
LHS 3003	14 56 38.0	-28 09 48	0.97 (0.04)	1	M7
Gl 570D	14 57 15.0	-21 21 51	1.14 (0.02)	4	T8
TVM 513-46546	15 01 08.3	+22 50 02	0.04 (0.11)	6	M8.5
2MASSW J1507-16	15 07 47.6	-16 27 38	0.59 (0.39)	2	L5 ^c
2MASSW J1523+30	15 23 22.6	+30 14 56	-1.35 (0.05)	4	L8
SDSS 1624+00	16 24 14.4	+00 29 16	...		T6
2MASSW J1632+19	16 32 29.1	+19 04 41	-1.20 (0.14)	3	L7.5
SDSS 1750+17	17 50 33.0	+17 59 04	...		T3.5
SDSS 2249+00	22 49 53.5	+00 44 04	...		L5
SDSS 2255-00	22 55 29.1	-00 34 33	...		M8.5

NOTE.—Units of right ascension are hours, minutes, and seconds, and units of declination are degrees, arcminutes, and arcseconds.

^a Parallaxes for distance moduli are from the following: (1) van Altena, Lee, & Hoffleit 1994. (2) C. Dahn 2000 (private communication reported by Kirkpatrick et al. 2000); (3) C. Dahn et al. 2000; (4) M. A. C. Perryman et al. 1997; (5) C. Dahn 1999 (private communication reported by Reid et al. 2001b); and (6) C. G. Tinney et al. 1995.

^b Spectral types are from G02 except where otherwise noted.

^c Spectral type from Kirkpatrick et al. 2000.

photometry with the spectral sequence presented in a companion paper by Geballe et al. (2002, hereafter G02); we also discuss the correlations between colors, and we compare the $K-L'$ and $K-M'$ colors of the L and T dwarfs with model predictions. Conclusions are given in § 6.

2. THE SAMPLE

Most of the sample comprises L and T dwarfs identified from SDSS (York et al. 2000) and 2MASS (Beichman et al. 1998). G02 describe the selection criteria for candidate L and T dwarfs culled from the SDSS photometric catalog. The sample presented here consists of both new and previously reported SDSS dwarfs, as well as other published cool dwarfs. This work is primarily concerned with the infrared colors of L and T dwarfs, but late-M dwarfs are included to define a blue edge to the sequences under study.

Table 1 lists the 58 dwarfs in the sample. Names and coordinates are given in the first three columns. Throughout this paper, we abbreviate the names of the DENIS, 2MASS, and SDSS objects by giving the survey acronym followed by the first four digits of right ascension and the sign and first two digits of declination. Note that Gl 570D is also known as 2MASSW J1457150–212148 and 2MASSW J1523+30 is also known as Gl 584C. The fourth column of Table 1 lists the distance moduli, where available, derived from sources as given in the table. The spectral types are listed in the sixth column.

Of the 12 M dwarfs in the sample, 11 have previously published spectral types. The one new SDSS M dwarf is classified as M8.5 by G02 on the basis of near-infrared water band indices. There are 29 L dwarfs in the sample. One is the prototype GD 165B (Becklin & Zuckerman 1988), another is Kelu-1 (Ruiz et al. 1997), three are from DENIS (Delfosse et al. 1997), 13 are from 2MASS (Kirkpatrick et al. 2000), and 11 are from SDSS (Fan et al. 2000; G02). G02 have classified all but four of these L dwarfs based on near-infrared spectral indices; the classification scheme is consistent with the optical/red schemes proposed by Kirkpatrick et al. (1999b) and Martín et al. (1999b), at least for spectral types L0 to around L6 (see discussion in G02). The spectral types of the four L dwarfs not classified by us have been taken from Kirkpatrick et al. (2000). There are 17 T dwarfs in the sample. One is the prototype Gl 229B (Nakajima et al. 1995), 11 are from SDSS, and five from 2MASS. G02 have classified all of these objects using near-infrared spectra.

3. PHOTOMETRIC DATA

3.1. Instrumentation

All new photometric data were obtained at the 3.8 m UKIRT on Mauna Kea, over the period 1999 June to 2001

May. Two cameras were used: UFTI, which has filters covering the region 0.85–2.4 μm and a plate scale of 0''.091 pixel⁻¹; and IRCAM, which has filters covering the region 1.15–4.9 μm and a plate scale of 0''.081 pixel⁻¹. The IRCAM field of view is 20''.7; UFTI was used in single-quadrant readout mode resulting in a field of view of 46''.6. UFTI contains a nonstandard Z filter. Both cameras contain Mauna Kea Observatory Near Infrared (MKO-NIR) J, H, and K filters. IRCAM also contains MKO-NIR L' and M' filters. The MKO-NIR system matches the near-infrared atmospheric windows, thereby producing more accurate photometry than previous filter systems and easing comparison of photometry between observatories (Simons & Tokunaga 2001; Tokunaga & Simons 2001). The half-power wavelength ranges of the filters are given in Table 2. These bandwidths reflect the transmission profiles of the filters at cold (instrument) temperatures convolved with the telescope optics and the Mauna Kea atmospheric transmission; the response of the detectors is flat across each filter bandpass and has not been included. The filter profiles are shown in Figure 1. To compare these profiles with those of other commonly used filters, see for example Bessell & Brett (1988).

The filters differ from the previous “UKIRT” system filters; transformations between the UKIRT JHK system and the MKO-NIR system for stars as cool as L dwarfs are given by Hawarden et al. (2001).¹⁵ These transformations cannot be applied to the colors of T dwarfs because of their very structured flux distributions within the filter bandpasses, and T dwarf colors must be transformed by convolving the flux distributions with the filter profiles, as described in § 3.3. The filter profiles and calibrated flux distributions for M, L, and T dwarfs can be obtained from the authors upon request. The photometric system used in this paper is calibrated by adopting zero magnitude at all wavebands for Vega; an infrared spectrum of Vega is also available on request. Note that different photometric systems produce significantly different infrared magnitudes: at JHK for L dwarfs the differences between for example the MKO-NIR and UKIRT, or MKO-NIR and 2MASS, magnitudes, are ~5%; for T dwarfs the difference at K is ~10%, at H ~5% and at J ~30%. At L' and M', T dwarf magnitudes can vary by ~20% depending on the filter set used; this is discussed further in § 5.3.

3.2. Observations

Table 3 lists the UKIRT Z magnitudes and dates of observation for 42 dwarfs in the sample. To calibrate the

¹⁵ See also http://www.jach.hawaii.edu/JACpublic/UKIRT/astronomy/calib/fs_newJHK.html.

TABLE 2
FILTER BANDPASSES

Filter Name	50% Cut-On Wavelength (μm)	50% Cut-Off Wavelength (μm)	Installed in Camera
UKIRT Z.....	0.851	1.056	UFTI
MKO J.....	1.165	1.329	UFTI, IRCAM
MKO H.....	1.487	1.780	UFTI, IRCAM
MKO K.....	2.027	2.362	UFTI, IRCAM
MKO L'.....	3.429	4.107	IRCAM
MKO M'.....	4.572	4.801	IRCAM

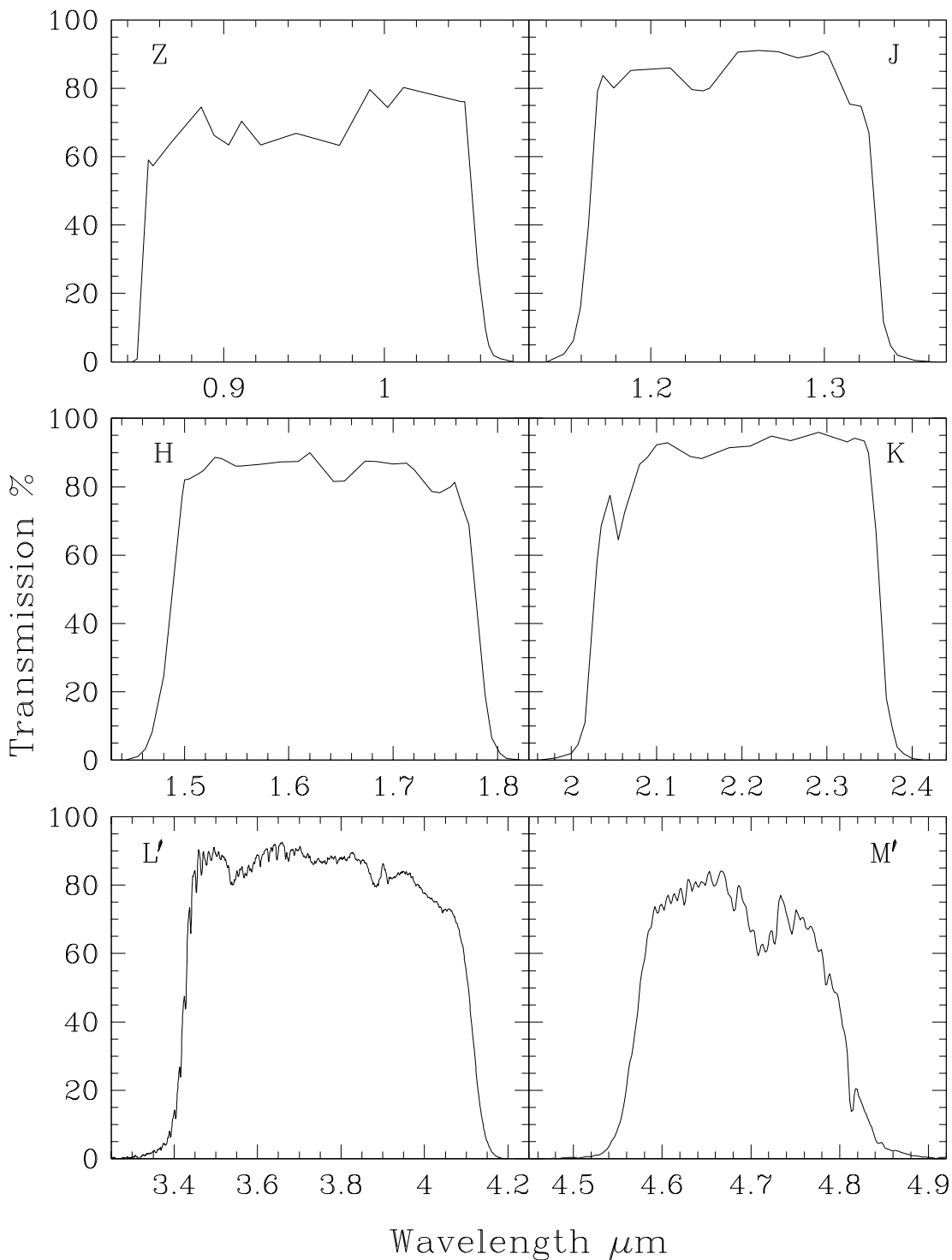


FIG. 1.—Profiles of filters at camera temperature and convolved with atmospheric and telescope transmission

nonstandard Z photometry, we derived transformations between the SDSS z' , Cousins I , UKIRT J and Z filters using A0 stars, which are defined as having zero color, and provisional z' standards (Krisciunas, Margon, & Szkody 1998). In doing so, we transformed the z' magnitudes from the SDSS AB photometric system to a colorless Vega-based system (z^\dagger) using the equation

$$z^\dagger = z' - 0.572$$

(see Table 8 of Fukugita et al. (1996)). The derived transformations are

$$\begin{aligned} Z_{\text{UFTI}} &= z^\dagger - (0.34 \pm 0.03)(I_C - z^\dagger), \\ Z_{\text{UFTI}} &= z^\dagger - (0.21 \pm 0.03)(z^\dagger - J_{\text{UKIRT}}). \end{aligned}$$

The 5% errors in the Z magnitudes are usually dominated by the calibration error. The Z filter provides color information where the flux distribution is rapidly rising for L and T dwarfs, and it is useful for calibrating both red

TABLE 3
UKIRT UFTI Z PHOTOMETRY

Name	$Z \pm 0.05$ (mag)	Date	Name	$Z \pm 0.05$ (mag)	Date
BRI 0021–0214	13.27	2000 Dec 05	2MASS J1047	17.39	2000 Dec 07
2MASS J0028+15	18.50	2001 Jan 14, 2000 Dec 05	LHS 292	9.76	2000 Dec 04
SDSS 0032+14	18.25	2000 Oct 12	LHS 36	8.11	2000 Mar 03, 2000 Dec 04
2MASSW J0036+18	14.11	2000 Dec 05	DENIS-P J1058	15.76	2000 Dec 04
SDSS 0107+01	17.33	2000 Oct 12	LHS 2347	13.96	2000 Dec 04, 1999 Dec 30
SDSS 0151+12	18.09	2000 Dec 05	LHS 2397a	13.13	2000 Dec 04, 1999 Dec 30
LHS 11	8.15	2000 Dec 04	LHS 315	7.17	1999 Dec 30
DENIS-P J0205–11AB	16.01	2000 Dec 04	2MASSW J1217	17.56	2000 Dec 07
SDSS 0207+00	18.71	2000 Dec 05	2MASSW J1225	16.77	2001 Feb 03
SDSS 0236+00	17.54	2000 Dec 04	DENIS-P J1228AB	16.01	2000 Dec 04
2MASSW J0328+23	18.06	2000 Dec 05	LHS 333AB	7.87	1999 Dec 30
SDSS 0423–04	15.98	2000 Oct 18	SDSS 1254	16.40	2000 Mar 02
SDSS 0539–00	15.60	2000 Mar 14	Kelu-1	15.00	2000 Mar 02
2MASSW J0559–14	15.55	2000 Oct 18	SDSS 1346	17.73	1999 Jun 20
2MASS J0746+20AB	13.11	2000 Dec 04	LHS 2924	13.35	1999 Aug 24
SDSS 0830+48	16.86	2000 Dec 04	Gl 570D	16.74	2000 Feb 01
SDSS 0837–00	18.59	2000 Mar 02	2MASSW J1523	17.60	2000 Mar 14
2MASSs J0850+10AB	18.15	2001 Jan 14	SDSS 1624	17.32	1999 Jun 20
SDSS 0857+57	16.52	2000 Dec 04	2MASSW J1632	17.52	2000 Feb 01
2MASSW J0929+34	18.38	2000 Dec 07	SDSS 2249	18.24	2000 Dec 04
SDSS 1021–03	17.66	2000 Mar 14	SDSS 2255	17.00	2000 Sep 23

spectra and the short-wavelength end of near-infrared spectra. Observations typically consisted of 120–250 s exposures, repeated three to five times with small telescope offsets between exposures. Flat fields were created through the night by median filtering these sets of dithered exposures. (Flat fields were created for all filter and instrument combinations using this technique.)

Table 4 lists the MKO-NIR *JHK* magnitudes, errors, camera selection, and date of observation for 34 dwarfs. The data were calibrated using UKIRT faint standards appropriately transformed onto the MKO-NIR system (Hawarden et al. 2001). No color terms could be detected between the cameras. Observations typically consisted of five 60 s exposures, with small telescope offsets between each exposure.

Table 5 lists the magnitudes and dates of observation for 21 dwarfs observed at *L'* and four dwarfs (two *L*, two *T*) observed at *M'*. All data were obtained using IRCAM and calibrated using UKIRT bright standards, for which no transformations are required between the UKIRT and MKO *L'* and *M'* systems. The *M'* data were obtained over two consecutive dry nights. At these wavelengths the sky background is high and exposure times have to be short. Typically, each *L'* exposure consisted of 100 co-added 0.2 s integrations, and each *M'* exposure comprised 75 co-adds of 0.12 s integrations. The telescope was offset slightly between exposures, adjacent pairs of frames were subtracted to remove the rapidly varying and high background, and every four pairs of differenced images were combined and divided by a flat field. This process was repeated until sufficient signal-to-noise was achieved. For targets with *L* \sim 11–13, total integration times of 1–30 minutes were required to achieve 5% photometry. For objects with *M'* \sim 12, about 1.3 hr of integration were required for 10% photometry. (Overhead is about a factor of 2 at these wavelengths.) These data are the first accurate *M*-band measurements of *L* and *T* dwarfs. The only previously published *M*-band

measurement is for Gl 229B, for which Matthews et al. (1996) obtained 7 ± 3 mJy, or $10.9 \pm \sim 0.5$ mag.

Bailer-Jones & Mundt (2001) have reported variability at the 5% level in the *I*-band for *M* and *L* dwarfs, which they suggest is due to dust formation. We have repeat observations for very few of our targets. Three dwarfs have two sets of *JHK* measurements: the *L* dwarfs SDSS 0107+00, SDSS 0830+48, and SDSS 1326–00. Observations of the first two objects repeated to better than 3%, and the last repeated well at *J*, but at *H*, and *K* the values differed by 9%, which may not be significant.

The image quality during our runs was characterized by seeing of $\text{FWHM} = 0''.4\text{--}1''.0$. No new, close (within a few arcseconds), candidate companions were resolved for any of our targets, to a 2σ detection limit of $H \approx 20.5$. Distant objects in the fields have not yet been followed up.

3.3. Synthesized Photometry

For some of the dwarfs listed in Table 1 we have synthesized MKO-NIR photometry by transforming data obtained with the previous UKIRT filter system or by convolving flux-calibrated spectra with the MKO-NIR bandpass profiles. We derived the MKO-NIR *JHK* magnitudes of three *M4*–*M5* dwarfs (LHS 11, LHS 315, and LHS 333AB) from their respective UKIRT system magnitudes using the transformations of Hawarden et al. (2001). We synthesized MKO-NIR *JHK* magnitudes for several late-*M*, *L*, and *T* dwarfs using the bandpass profiles and flux-calibrated spectra from Leggett et al. (2000a, 2001), and G02. We calibrated the synthetic magnitudes by convolving the energy distribution of Vega with the bandpass profiles and by assigning zero magnitude to Vega in each bandpass. The objects listed in Table 1 for which synthetic *JHK* magnitudes were derived are the *M* dwarfs LHS 36, LHS 292, LHS 3003, TVLM 513–46546, and BRI 0021–0214; the *L* dwarfs 2MASP J0345+25, Kelu-1, DENIS-P J1058–15, GD 165B, and DENIS-P J1228–15AB; and the *T* dwarfs

TABLE 4
UKIRT MKO-NIR *JHK* PHOTOMETRY

Name	<i>J</i>	<i>H</i>	<i>K</i>	Error (mag)	Camera	Date
2MASS J0028+15	16.65	15.56	14.57	0.05	UFTI	2001 Jan 14
SDSS 0032+14	16.58	15.66	14.99	0.05	UFTI	2000 Sep 21
2MASSW J0036+18	12.32	11.63	11.03	0.03	UFTI	2000 Dec 05
SDSS 0107+00	15.75	14.56	13.58	0.03	UFTI	1999 Oct 17, 2001 Jan 24
SDSS 0151+12	16.25	15.54	15.18	0.05	UFTI	2000 Sep 21
DENIS-P J0205-11AB	14.43	13.61	12.99	0.05	IRCAM	1999 Sep 19
SDSS 0207+00	16.63	16.66	16.62	0.05	UFTI	2000 Dec 05
SDSS 0236+00	16.01	15.16	14.54	0.05	UFTI	1999 Oct 27
2MASSW J0310+16	15.88	14.91	14.18	0.03	UFTI	2000 Dec 05
2MASSW J0328+23	16.35	15.47	14.87	0.03	UFTI	2000 Dec 05
SDSS 0423-04	14.30	13.51	12.96	0.03	UFTI	2000 Oct 13
2MASSW J0559-14	13.57	13.64	13.73	0.03	UFTI	2000 Oct 13
2MASS J0746+20AB	11.64	11.01	10.43	0.03	IRCAM	2000 Dec 06
2MASS J0825+21	14.89	13.81	12.93	0.03	UFTI	2001 Jan 23
SDSS 0830+48	15.22	14.40	13.68	0.03	IRCAM	2000 Nov 19, 2000 Dec 06
2MASSs J0850+10AB	16.20	15.21	14.35	0.03	UFTI	2000 Dec 07
SDSS 0857+57	14.80	13.80	12.94	0.03	IRCAM	2000 Dec 06
SDSS 0926+58	15.47	15.42	15.50	0.03	UFTI	2001 Jan 23
2MASSW J0929+34	16.69	15.62	14.73	0.03	UFTI	2000 Dec 07
2MASS J1047+21	15.46	15.83	16.20	0.03	UFTI	2000 Dec 07
SDSS 1110+01	16.12	16.22	16.05	0.05	UFTI	2001 Feb 18
2MASSW J1217-03	15.56	15.98	15.92	0.03	UFTI	2000 Dec 07
2MASSW J1225-27	14.88	15.17	15.28	0.03	UFTI	2000 Dec 07
SDSS 1257-01	15.64	14.68	14.06	0.03	UFTI	2000 Mar 14
SDSS 1314-00	16.33	15.84	15.28	0.05	UFTI	2000 Mar 14
SDSS 1326-00	16.19	15.06	14.13	0.05	UFTI	2000 Mar 14, 2001 Jan 23
2MASSW J1439+19	12.66	12.05	11.47	0.03	UFTI	2001 Jan 23
SDSS 1446+00	15.56	14.59	13.80	0.05	UFTI	2000 Mar 14
2MASSW J1507-16	12.70	11.90	11.29	0.03	UFTI	2001 Jan 23
2MASSW J1523+30	15.95	15.05	14.35	0.05	UFTI	2000 Mar 14
2MASSW J1632+19	15.77	14.68	13.97	0.05	UFTI	2000 Feb 01
SDSS 1750+17	16.14	15.94	16.02	0.05	UFTI	2001 Feb 18
SDSS 2249+00	16.46	15.42	14.43	0.05	UFTI	2001 Jan 16
SDSS 2255-00	15.50	14.80	14.28	0.05	UFTI	2000 Sep 21

TABLE 5
UKIRT IRCAM *L'* AND *M'* PHOTOMETRY

NAME	<i>L'</i> (error) (mag)	Date	<i>M'</i> (error) (mag)	Date
2MASSW J0036+18	10.08 (0.05)	2001 Jan 20	10.35 (0.05)	2001 Jan 21, 2001 Jan 22
SDSS 0107+00	12.06 (0.07)	2000 Nov 20
2MASSW J0310+16	12.54 (0.05)	2001 Feb 18
SDSS 0423-04	11.45 (0.05)	2000 Nov 20
SDSS 0539+00	11.32 (0.05)	2000 Dec 06
2MASSW J0559-14	12.14 (0.05)	2000 Nov 20	12.15 (0.15)	2001 Jan 21, 2001 Jan 22
2MASS J0746+20AB	9.67 (0.03)	2000 Dec 06
SDSS 0830+48	11.98 (0.05)	2000 Dec 06
2MASS J0825+21	11.53 (0.03)	2001 May 23
2MASSs J0850+10AB	12.94 (0.05)	2001 Jan 20
SDSS 0857+57	11.31 (0.05)	2000 Dec 06	11.50 (0.10)	2001 Jan 21
LHS 2397a	10.03 (0.02)	2001 Jan 20
2MASSW J1217-03	13.96 (0.05)	2001 May 23
2MASSW J1225-27	13.22 (0.08)	2001 Jan 20
SDSS 1254-01	12.25 (0.05)	2000 Mar 03	12.65 (0.20)	2001 Jan 21, 2001 Jan 22
LHS 2924	10.12 (0.03)	2000 Mar 03, 2001 Jan 20
2MASSW J1439+19	10.80 (0.05)	2001 Jan 20
2MASSW J1507-16	9.98 (0.03)	2001 Jan 20
2MASSW J1523+30	12.86 (0.05)	2001 May 23
SDSS 1624+00	13.60 (0.04)	1999 Sep 20, 2001 May 23
2MASSW J1632+19	12.54 (0.05)	2000 May 15

TABLE 6
INFRARED MAGNITUDES AND COLORS, SORTED BY SPECTRAL TYPE

Name	Type	M_K	$Z-J$	J	$J-K$	$J-H$	$H-K$	K	$K-L'$	$L-M'$
LHS 315 ^a	M4	8.03	0.67	6.50	0.85	0.51	0.34	5.65	0.41	...
LHS 333AB ^a	M4	7.87	0.88	6.99	0.91	0.50	0.41	6.08	0.45	...
LHS 11 ^a	M5	8.41	0.68	7.47	0.82	0.48	0.35	6.65	0.33	...
LHS 2347	M5	...	0.94	13.02	0.94	0.52	0.42	12.08
LHS 36 ^b	M6	9.17	1.07	7.03	0.97	0.55	0.43	6.06	0.35	...
LHS 292 ^b	M6.5	9.67	0.83	8.92	0.97	0.53	0.44	7.95	0.50	...
LHS 3003 ^b	M7	9.90	...	9.94	1.01	0.51	0.50	8.93	0.50	...
LHS 2397a	M8	9.92	1.30	11.83	1.14	0.57	0.57	10.69	0.66	...
SDSS 2255-00	M8.5	...	1.50	15.50	1.22	0.70	0.52	14.28
TVLM 513-46546 ^b	M8.5	10.73	...	11.76	1.07	0.58	0.49	10.69	0.65	...
LHS 2924	M9	10.55	1.44	11.91	1.19	0.64	0.55	10.72	0.60	...
BRI 0021-0214 ^b	M9.5	10.11	1.54	11.73	1.20	0.63	0.57	10.53	0.75	...
2MASS J0746+20AB	L1	9.99	1.47	11.64	1.21	0.63	0.58	10.43	0.76	...
2MASS J0345+25 ^b	L1	10.48	...	13.84	1.18	0.63	0.54	12.66	0.65	...
2MASS J1439+19 ^c	L1	10.69	...	12.66	1.19	0.61	0.58	11.47	0.67	...
SDSS 1314-00	L2	16.33	1.05	0.49	0.56	15.28
2MASS J0028+15	L3	...	1.85	16.65	2.08	1.09	0.99	14.57
DENISP J1058-15 ^b	L3	11.33	1.64	14.12	1.57	0.84	0.74	12.55	0.93	...
GD 165B ^b	L3	11.60	...	15.64	1.55	0.89	0.66	14.09	1.16	...
Kelu-1 ^b	L3	10.38	1.77	13.23	1.45	0.78	0.67	11.78	1.00	...
2MASS J0036+18	L4	11.33	1.79	12.31	1.29	0.69	0.60	11.03	0.95	-0.27
2MASS J1507-16 ^c	L5	11.88	...	12.70	1.41	0.80	0.61	11.29	1.31	...
SDSS 0539-00	L5	...	1.75	13.85	1.45	0.81	0.64	12.40	1.08	...
SDSS 1257-01	L5	15.64	1.58	0.96	0.62	14.06
SDSS 1446+00	L5	15.56	1.76	0.97	0.79	13.80
SDSS 2249+00	L5	...	1.78	16.46	2.03	1.04	0.99	14.43
DENIS-P J0205-11AB	L5.5	11.86	1.58	14.43	1.44	0.82	0.62	12.99	1.55	...
SDSS 0107+00	L5.5	...	1.58	15.75	2.17	1.19	0.98	13.58	1.52	...
SDSS 1326-00	L5.5	16.19	2.06	1.13	0.93	14.13
2MASS J0825+21	L6	12.45	...	14.89	1.96	1.08	0.88	12.93	1.40	...
2MASS J0850+10AB ^c	L6	11.88	1.95	16.20	1.85	0.99	0.86	14.35	1.41	...
DENIS-P J1228-15AB ^b	L6	11.42	1.73	14.28	1.57	0.88	0.69	12.71	1.29	...
SDSS 0236+00	L6.5	...	1.53	16.01	1.47	0.85	0.62	14.54
2MASS J1632+19	L7.5	12.77	1.75	15.77	1.80	1.09	0.71	13.97	1.43	...
2MASS J0929+34 ^c	L8	...	1.69	16.69	1.96	1.07	0.89	14.73
2MASS J1523+30	L8	13.00	1.65	15.95	1.60	0.90	0.70	14.35	1.49	...
SDSS 0032+14	L8	...	1.67	16.58	1.59	0.92	0.67	14.99
SDSS 0857+57	L8	...	1.72	14.80	1.86	1.00	0.86	12.94	1.63	-0.19
SDSS 0830+48	L9	...	1.64	15.22	1.54	0.82	0.72	13.68	1.70	...
2MASS J0310+16	L9	15.88	1.70	0.97	0.73	14.18	1.64	...
2MASS J0328+23	L9.5	...	1.71	16.35	1.48	0.88	0.60	14.87
SDSS 0423-04	T0	...	1.68	14.30	1.34	0.79	0.55	12.96	1.51	...
SDSS 0837-00	T0.5	...	1.69	16.90	0.92	0.69	0.23	15.98
SDSS 0151+12	T1	...	1.84	16.25	1.07	0.71	0.36	15.18
SDSS 1254-01	T2	...	1.74	14.66	0.82	0.53	0.29	13.84	1.59	-0.40
SDSS 1021-03	T3	...	1.78	15.88	0.62	0.47	0.15	15.26
SDSS 1750+17	T3.5	16.14	0.12	0.20	-0.08	16.02
2MASS J0559-14	T4.5	...	1.98	13.57	-0.16	-0.07	-0.09	13.73	1.59	-0.01
SDSS 0207+00	T4.5	...	2.08	16.63	0.01	-0.03	0.04	16.62
SDSS 0926+58	T4.5	15.47	-0.03	0.05	-0.08	15.50
2MASS J1225-27	T6	...	1.89	14.88	-0.40	-0.29	-0.11	15.28	2.06	...
GI 229B ^d	T6	15.55	2.17	14.01	-0.35	-0.35	0.00	14.36	2.14	...
SDSS 1110+01	T6	16.12	0.07	-0.10	0.17	16.05
SDSS 1346-00 ^b	T6	...	2.24	15.49	-0.24	-0.35	0.11	15.73
SDSS 1624+00 ^b	T6	...	2.12	15.20	-0.41	-0.28	-0.13	15.61	2.01	...
2MASS J1047+21	T6.5	...	1.93	15.46	-0.74	-0.37	-0.37	16.20
2MASS J1217-03	T8	...	2.00	15.56	-0.36	-0.42	0.06	15.92	1.96	...
GI 570D	T8	16.66	1.92	14.82	-0.70	-0.46	-0.24	15.52	2.54	...

NOTE.—Uncertainty in spectral type is ~ 0.5 subclasses; error in M_K is $\sim 10\%$ except for objects with more uncertain parallaxes, see Table 1; error in colors is typically $\sim 5\%$ except for $L-M'$; see Table 5.

^a JHK on MKO system derived from transformations given in Hawarden et al. 2001.

^b JHK magnitudes synthesized from flux-calibrated spectrum.

^c L spectral type taken from Kirkpatrick et al. 2000.

^d $ZJHKL$ magnitudes synthesized from flux-calibrated spectrum.

SDSS 1346–00 and SDSS 1624+00. For the T dwarf Gl 229B we synthesized all of the $ZJHKL$ magnitudes using the flux-calibrated spectrum of Leggett et al. (1999) (a recalibrated combination of the spectra of Geballe et al. 1996 and Oppenheimer et al. 1998).

3.4. Observed Colors

Table 6 lists all the new and transformed $ZJHKL$ colors for the sample, sorted by spectral type. Absolute K magnitudes are given for objects with published parallax measurements.

Table 6 also includes the previously published MKO-NIR colors of SDSS 0539–00, SDSS 0837–00, SDSS 1021–03, SDSS 1254–01 (Leggett et al. 2000b), and Gl 570D (Geballe et al. 2001). JHK photometry is listed for three UKIRT M-dwarf photometric standards (LHS 2347, LHS 2397a, and LHS 2924), obtained as part of a UKIRT program to observe standards with the MKO filter set. Additional L' data for M dwarfs have been taken from Leggett (1992) and Leggett et al. (1998). Additional L' data for L dwarfs have been taken from Jones et al. (1996) for GD 165B, from Leggett et al. (1998) for Kelu-1 and from Leggett et al. (2001) for 2MASP J0345+25, DENIS-P J0205–11AB, DENIS-P J1058–15 and DENIS-P J1228–15AB. Some of these data were obtained with the UKIRT L' filter which cuts on slightly redder than the MKO-NIR filter. Although this is significant for late L dwarfs and T dwarfs, as we discuss below, for these earlier type objects the effect is less than the uncertainties in the published magnitudes.

4. LUMINOSITIES AND EFFECTIVE TEMPERATURES

It is useful to estimate effective temperatures for our sample in order to interpret the trends seen in our observed colors. To do so we use the observed luminosities, as the theoretical determinations of radius and luminosity for low-mass stars and brown dwarfs are reasonably robust and independent of the atmospheric models. T_{eff} can therefore be derived from integrated luminosity with reasonable assumptions for radius.

Figure 2 shows M_K versus $J-K$ (left) and $K-L'$ (right) for those dwarfs in our sample with published parallaxes. In the left panel, we have labeled the faintest L and T dwarfs; in the right panel, we have labeled the known binaries and Kelu-1, which is superluminous but for which *Hubble Space Telescope* observations show no resolved companion (Martín, Brandner, & Basri 1999a). DENIS-P J1228–15AB, and DENIS-P J0205–11AB are composed of identical pairs of L dwarfs (Martín et al. 1999a; Leggett et al. 2001). 2MASS J0746+20AB consists of a pair of similar early L dwarfs, and 2MASS J0850+10AB consists of an L dwarf and probably a T dwarf (Reid et al. 2001b).

$J-K$ reddens at first with decreasing M_K , or decreasing effective temperature, then becomes bluer as the K -band CH_4 and H_2O absorptions become stronger (see for example the spectra presented in G02). $K-L'$ increases approximately monotonically in this figure and spectral types are indicated along the top of the right-hand panel. As we show later, the near-infrared colors of L and T dwarfs do show some scatter with spectral type and more trigonometric parallaxes must be obtained before we can adequately

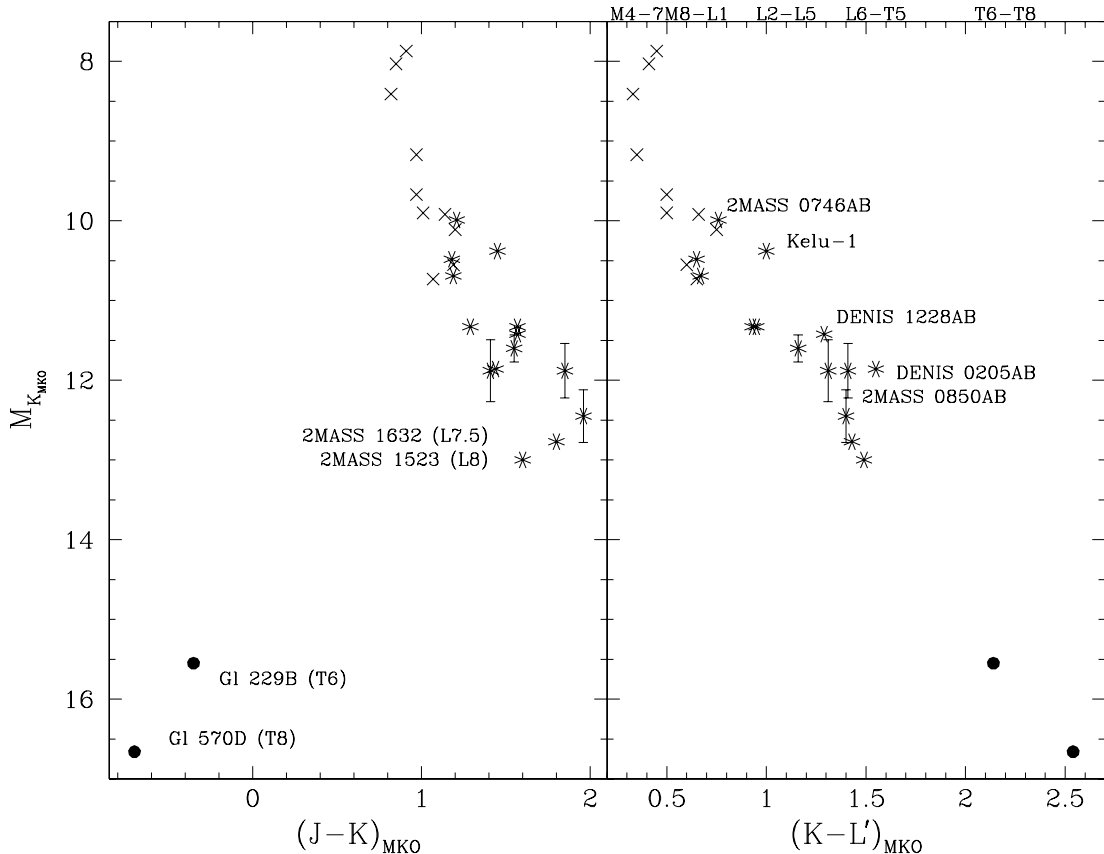


FIG. 2.—Plots of absolute K magnitude vs. $J-K$ (left) and $K-L'$ (right) for M dwarfs (crosses), L dwarfs (asterisks), and T dwarfs (filled circles). Error bars are shown for dwarfs with absolute magnitude errors greater than 0.15 mag.

TABLE 7
LUMINOSITY AND TEMPERATURE

Name	Type	BC _K	log ₁₀ L/L _☉	T _{eff} (K)
LHS 36	M6	2.97	-2.97	2650-2850
LHS 292	M6.5	2.95	-3.16	2500-2700
LHS 3003	M7	3.03	-3.28	2400-2650
TVLM 513-46546	M8.5	3.13	-3.65	2000-2250
BRI 0021-0214	M9.5	3.17	-3.43	2200-2450
2MASP J0345+25	L1	3.20	-3.59	2050-2350
2MASS J0746+20AB	L1	3.26	-3.40	1900-2200 ^a
Kelu-1	L3	3.27	-3.57	2100-2350
DENIS-P J1058-15	L3	3.31	-3.98	1700-1950
GD 165B	L3	3.27	-4.06	1650-1850
2MASSW J0036+18	L4	3.34	-3.97	1700-1950
DENIS-P J0205-11AB	L5.5	3.18	-4.12	1400-1600 ^a
DENIS-P J1228-15AB	L6	3.27	-4.00	1450-1650 ^a
2MASS J0825+21	L6	3.31	-4.40	1400-1600
2MASSW J1632+19	L7.5	3.19	-4.48	1350-1550
2MASSW J1523+30	L8	3.17	-4.57	1250-1500
Gl 229B	T6	2.22	-5.21	870-1030
Gl 570D	T8	1.90	-5.53	784-824

^a Assuming equal contribution to luminosity from each component.

determine how these variations affect the infrared color-magnitude diagrams of brown dwarfs.

We have compiled the bolometric luminosities of 18 dwarfs in our sample for which both flux-calibrated spectra and parallaxes are available. The luminosities of the M to mid-L dwarfs are obtained from Leggett et al. (2000a, 2001); those of the T dwarfs Gl 229B and Gl 570D are from

Saumon et al. (2000) and Geballe et al. (2001), respectively. We have determined the luminosities of 2MASSW J0036+18 (L4), 2MASS J0825+21 (L6), 2MASSW J1523+30 (L8), and 2MASSW J1632+19 (L7.5), by summing their energy distributions from the red to the K band, interpolating the flux between the K band and the effective L' flux computed from our photometry, and assuming Rayleigh-Jeans curves longward of L'. Neither the interpolation between K and L' nor the Rayleigh-Jeans extrapolation is a correct assumption for T dwarfs, as there is CH₄ absorption shortward of L', and there are CH₄ and H₂O absorption bands between 6 and 8 μm (Burrows, Marley, & Sharp 1997). A correction to this simple approach was determined for Gl 229B by Leggett et al. (1999) using model atmospheres. Leggett et al. (2001) also used models to show that no correction is needed for dwarfs as late as mid L. Therefore, we adopt a correction for the 2MASS L7.5 and L8 dwarfs that is half that computed for Gl 229B, which amounts to a 5% adjustment to the total integrated luminosity.

Table 7 lists the names, spectral types, K-band bolometric corrections (BC_K), and bolometric luminosities (expressed as log₁₀ L/L_☉) for the 18 dwarfs. The uncertainties of the total measured fluxes are typically 5% and are usually dominated by the absolute calibration. These uncertainties correspond to errors in the computed BC_K and log₁₀ L/L_☉ of about 0.07 mag and 0.03 dex, respectively. The parallaxes of GD 165B and 2MASS J0825+21 are less well determined than those of the other dwarfs, so their bolometric luminosities are correspondingly less certain. Figure 3 shows BC_K versus J-K (left) and K-L' (right)

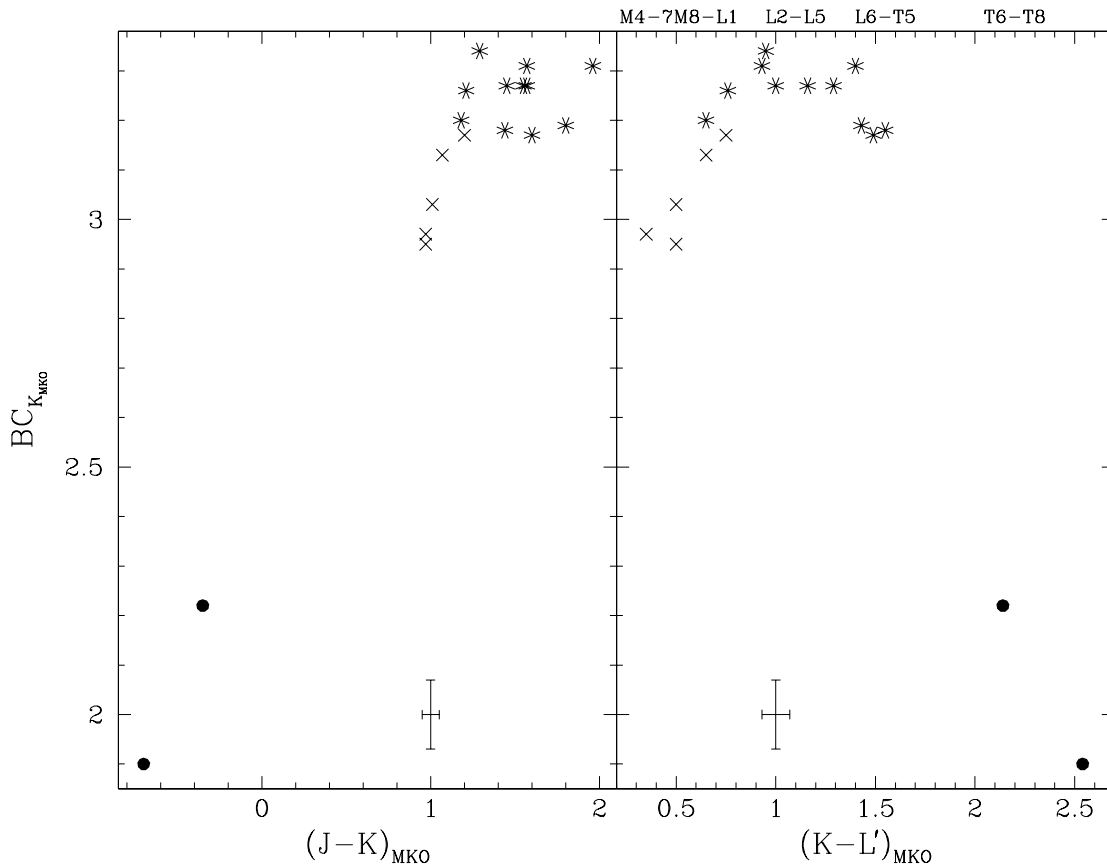


FIG. 3.—Plots of K-band bolometric correction vs. J-K (left) and K-L' (right) for M dwarfs (crosses), L dwarfs (asterisks), and T dwarfs (filled circles). A typical error bar is shown at the bottom of each panel.

(right) so that $M_{\text{bol}} (= BC_K + M_K)$ can be estimated for other dwarfs. The sample is too small to allow a polynomial fit to these data.

We used the relationship between T_{eff} and $\log_{10} L/L_{\odot}$ derived from the models of Chabrier et al. (2000) (see Fig. 12 of Leggett et al. 2001) to compute T_{eff} for 2MASSW J0036+18, 2MASSI J0825+21, 2MASSW J1523+30, and 2MASSW J1632+19, assuming that their ages lie in the range 0.1–10 Gyr. The computed values of T_{eff} for these dwarfs are listed in Table 7 along with previously published values for the other dwarfs (Geballe et al. 2001; Leggett et al. 2000a, 2001; Saumon et al. 2000). The range in T_{eff} listed for each dwarf reflects its uncertain age. The temperatures derived for the late-L dwarfs are consistent with the temperature at which CH_4 is expected to become more abundant than CO in brown dwarf photospheres (Lodders 1999); the appearance of CH_4 absorption features in both of the H and K bands is the defining spectral signature of a T dwarf (G02). A trend between spectral type and effective temperature is apparent in Table 7; however, as we show below, the JHK colors of L dwarfs show significant scatter with spectral type and more bolometric luminosities must be determined to confirm whether or not a unique value of T_{eff} is associated with each spectral type.

5. DISCUSSION OF INFRARED COLORS

5.1. Colors and Spectral Type

Figure 4 is a plot of $J-H$ (top), $J-K$ (middle), and $K-L'$ (bottom) versus spectral type for the dwarfs in our sample. The average uncertainties are represented by the error bars shown in the left of each panel. All the L and T dwarfs have been classified spectroscopically by G02 except for four L dwarfs whose types have been taken from Kirkpatrick et al. (2000); these four objects are shown as open triangles in the figure. There is good consistency between L spectral types assigned using red spectra by Kirkpatrick et al. and those assigned using near-infrared spectra by Geballe et al. for spectral types L0 to around L6; however, for the latest L types the schemes can differ by up to two subclasses.

At these wavelengths the principle opacity sources in the photospheres of cool dwarfs (with $2700 \gtrsim T_{\text{eff}} \gtrsim 800$ K) are H_2O at both the short and long wavelength edges of each of the JHK bands, CH_4 at 1.6–1.8, 2.2–2.4, and 3.1–3.6 μm (affecting H , K , and the blue edge of the L' band), pressure-induced H_2 at 1.8–3.0 μm (K) and CO at 2.3–2.4 and 4.4–5.0 μm (K and M'). Figure 15 in Burrows et al. (2001) shows absorption cross sections versus wavelength from the optical to the M band for all these species, and is a very useful reference. The features can be compared to our filter bandpasses shown in Figure 1.

T dwarfs (with $1300 \gtrsim T_{\text{eff}} \gtrsim 800$ K) become bluer in both $J-H$ and $H-K$ as T_{eff} decreases and the H - and K -band absorptions by CH_4 strengthen (G02). The trend toward bluer $J-K$ begins around spectral type L8. This result is consistent with the observations of G02 that CH_4 absorption is seen in the K -band spectra of the latest L dwarfs. Note that the blueward trend in $J-H$ slows between types T6 and T8. This behavior probably reflects the saturation of the CH_4 absorption in the H band (see the spectra presented in G02).

$K-L'$ generally increases through the M, L, and T classes but the increase slows for types around L6 through to T5. Noll et al. (2000) detect the onset of 3.3 μm absorp-

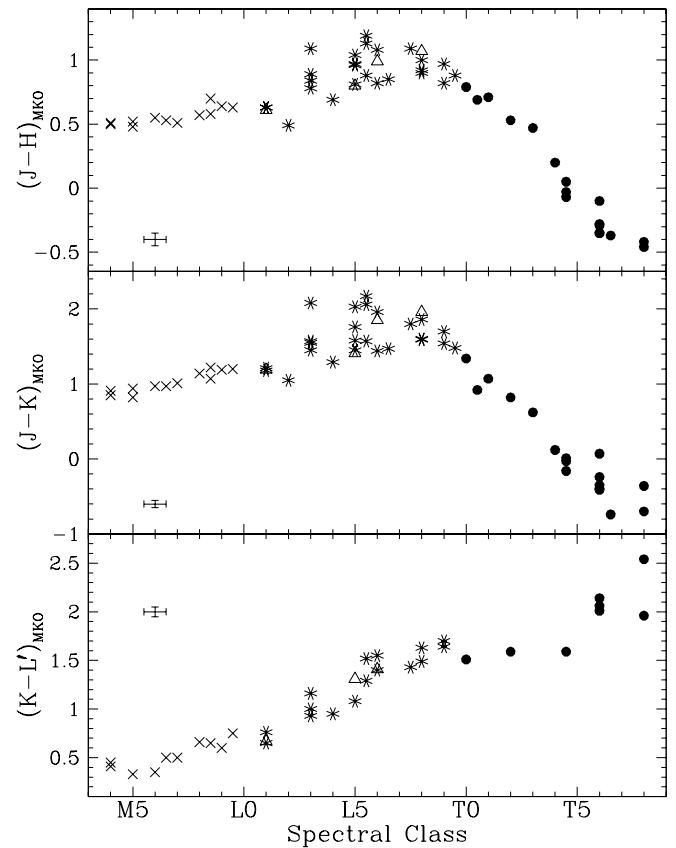


FIG. 4.—Plot of $J-H$ (top), $J-K$ (middle), and $K-L'$ (bottom) vs. spectral type for M dwarfs (crosses), L dwarfs (asterisks), and T dwarfs (filled circles), where spectral types are assigned by G02. In addition four L dwarfs are shown as open triangles for which spectral types are from Kirkpatrick et al. (2000).

tion by CH_4 (the fundamental band) for 2MASSI J0825+21 (L6) and 2MASSW J1507–16 (L5), and this feature is strong for T dwarfs as shown by the spectrum presented by Oppenheimer et al. (1998). This absorption band is included at the blue edge of our L' bandpass and so is probably slowing the increase in $K-L'$ for objects later than L6; tests with the Oppenheimer et al. L -band spectrum of Gl 229B show the effect to be $\gtrsim 0.2$ mag at T6. The more rapid rise in $K-L'$ at later types probably reflects the saturation of the CH_4 absorption.

The colors are well constrained among the late M dwarfs. However the JHK colors of the L dwarfs show significant scatter. The same phenomenon is seen in Figure 5 of Reid et al. (2001a). These spectral types have a range of effective temperature ($2200 \gtrsim T_{\text{eff}} \gtrsim 1300$ K) over which grain condensation is expected in the photosphere (Tsuji et al. 1996; Chabrier et al. 2000; Ackerman & Marley 2001; Allard et al. 2001). The brightness temperature spectra presented by Ackerman & Marley (2001) show that the near-infrared fluxes of L dwarfs may be strongly affected by dust cloud behavior. The absorbing dust is expected to heat the photosphere and consequently reduce the depth of the H_2O absorption bands (for the limiting cases of fully dusty and dust-free atmospheres compare Figures 8 and 14 in Allard et al. 2001). Table 6 shows that both $J-H$ and $H-K$ can vary by 0.2–0.3 mag among L dwarfs of the same type (repeat observations of two of the redder L dwarfs show good agreement, § 3.2, and so the reddening does not seem to be a temporary effect). One example of an apparently red

L dwarf is the L5 SDSS 2249+00, for which G02 find spectral types inferred separately from the H - and K -band indices that are discrepant by three subclasses, whereas these indices are consistent for the other L5 dwarfs. However there are also examples of L dwarfs with very different infrared colors but well-behaved spectral indices, such as the L3 dwarfs 2MASS J0028+15 and DENIS-P J1058-15. G02 find that the L subclasses correlate well with the depth of the H_2O absorption band at $1.5 \mu\text{m}$, although the K -band water features shows less sensitivity to spectral type. The scatter in color with L subclass may indicate varying dust properties caused by differences in metallicity (which affects dust abundance), age (which limits settling time), and rotational velocity (which may inhibit dust settling). A better understanding of the spectroscopic and photometric behavior of mid-L dwarfs will have to await detailed models with a full and accurate treatment of grain condensation.

The T dwarfs also show some scatter, in particular in $J-K$ and $K-L'$ for the latest T dwarfs. At these temperatures ($T_{\text{eff}} \sim 1000 \text{ K}$) grains are calculated to lie below the photosphere, and the absorption bands of H_2O and CH_4 are close to saturation (see G02). The scatter seen here may be due to variations in the strength of the pressure-induced H_2 opacity in the K -band, which is expected to be an important opacity source at these temperatures and is sensitive to gravity and metallicity (e.g., Borysow, Jorgensen, & Zheng 1997). Again, understanding this behavior must await more detailed photospheric models.

5.2. ZJHKL Color-Color Sequences

Figure 5 shows the $J-H$ versus $H-K$ diagram for our sample. The average photometric errors are represented by the error bars shown in the lower right-hand corner of the figure. The colors of the L and T dwarfs show some scatter as discussed in the previous section. Note that the early T dwarfs are not easily distinguished from M and L dwarfs by JHK photometry alone.

Figure 6 shows $J-K$ versus $Z-J$ (left) and $K-L'$ (right) for our sample. While $Z-J$ correlates well with $J-K$ for M dwarfs, it is almost constant ($Z-J \approx 1.8$) for L and T dwarfs. This behavior is caused by the balanced losses of flux in the Z and J bands from two very different sources of opacity. As T_{eff} decreases, increased absorption by the highly pressure-broadened $K I$ resonance doublet at 0.7665 and $0.7699 \mu\text{m}$ dominates the Z -band region of the spectrum (Tsuji, Ohnaka, & Aoki 1999; Burrows, Marley, & Sharp 2000; Liebert et al. 2000). At the same time, deepening absorption by the $1.15 \mu\text{m}$ and, to a lesser extent, the

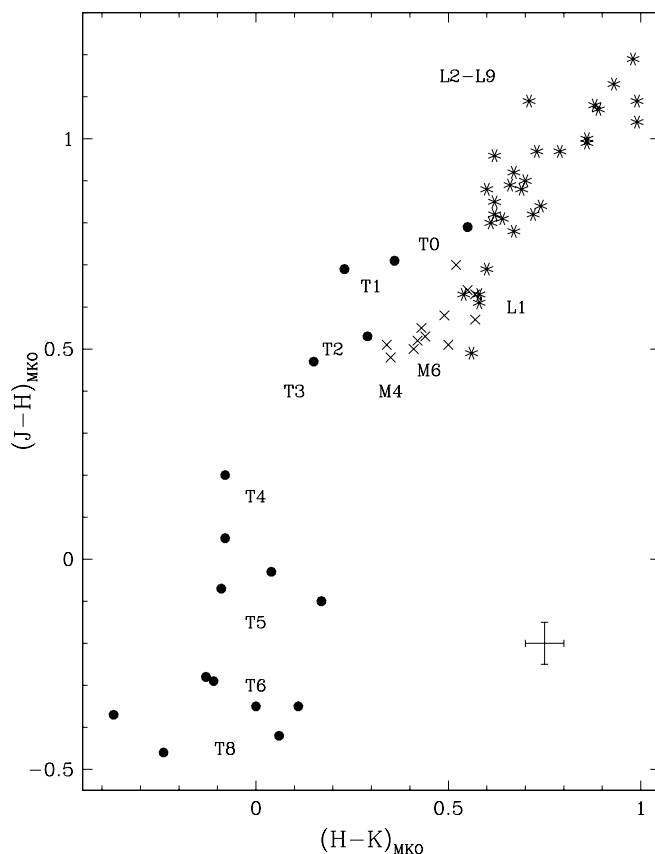


FIG. 5.—Color-color diagram of $J-H$ vs. $H-K$ diagram for M dwarfs (crosses), L dwarfs (asterisks), and T dwarfs (filled circles). The location by spectral type is indicated.

short wavelength wing of the $1.4 \mu\text{m}$ H_2O bands, reduces the emergent J -band flux. (See the spectra presented in G02 and the bandpasses shown in Fig. 1.) The strong $K I$ feature makes the use of a red continuum index problematical for classifying late L and T dwarfs (G02).

Good correlation exists between $J-K$ and $K-L'$ for types mid-M to mid-L and for the later T subclasses. The degeneracy of $K-L'$ between types L6 and T5 can probably be attributed to increasing absorption in both bandpasses, as described above in § 5.1.

5.3. KLM' : Discrepancy with Models

In Table 8 we summarize our observed $K-L'$ and $K-M'$ colors as a function of spectral type and estimated

TABLE 8
 $K-L'$, $K-M'$: MODEL COMPARISON

$K-L'$					$K-M'$				
TYPE	$\sim T_{\text{eff}}$ (K)	Observed	Calculated		TYPE	$\sim T_{\text{eff}}$ (K)	Observed	Calculated	
			Dusty ^a	Settled ^b				Dusty ^a	Settled ^b
L1.....	2100	0.7	1.0	...	L4.....	1800	0.7 ± 0.1	1.0	...
L8.....	1400	1.6	1.8	...	L8.....	1400	1.4 ± 0.1	2.0	...
T0.....	1300	1.5	2.1	...	T2.....	1300-1000	1.2 ± 0.2	2.1-3.3	...
T6.....	950	2.0	3.3	2.3	T4.5.....	1300-1000	1.6 ± 0.2	2.1-3.3	~ 3.0

^a Chabrier et al. (2000) for ages 0.1-10 Gyr, corresponding to $\log g \approx 4.2-5.4$

^b Burrows et al. (1997) for $\log g = 4.5-5.0$ corresponding to ages $\approx 0.3-1$ Gyr.

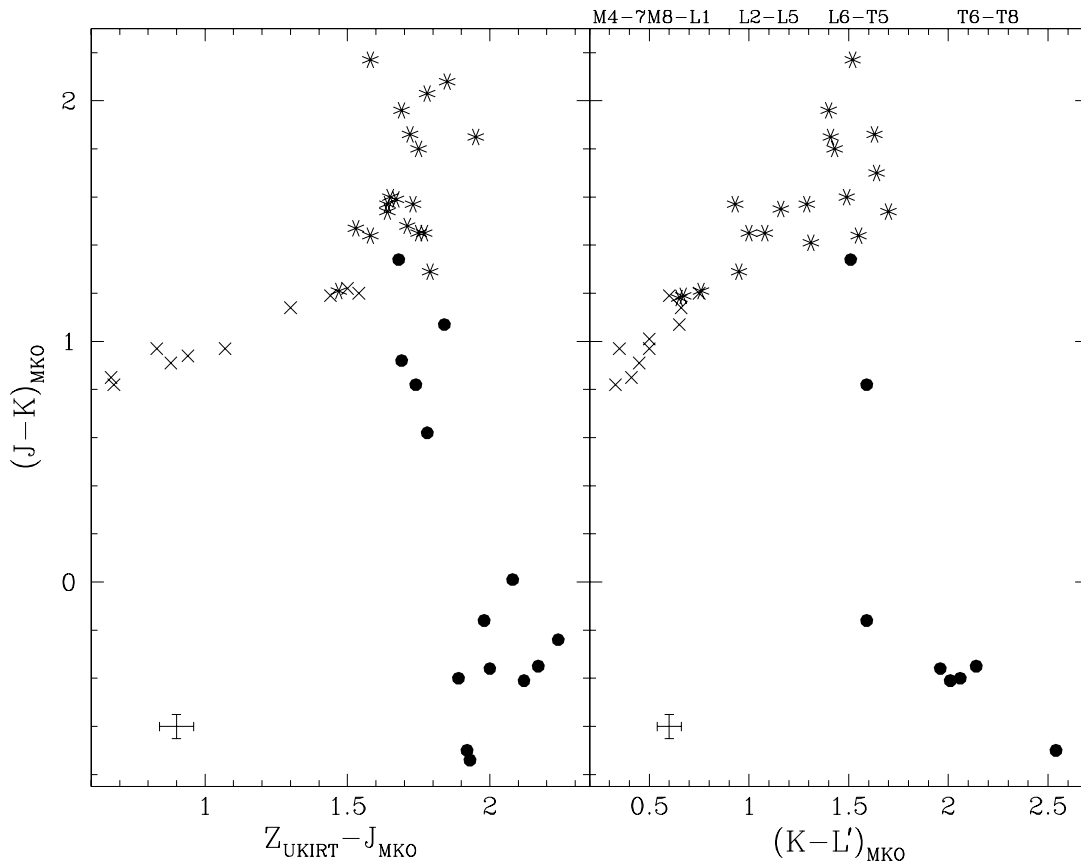


FIG. 6.—Color-color diagrams of $J-K$ vs. $Z-J$ (left) and $K-L'$ (right) for M dwarfs (crosses), L dwarfs (asterisks), and T dwarfs (filled circles)

effective temperature. We also compare the observed colors to those calculated by two models which handle grain condensation (dust) differently. These are the models of very low mass stars and brown dwarfs with dusty atmospheres by Chabrier et al. (2000), and the models of brown dwarfs in which dust is treated as if condensed below the photosphere by Burrows et al. (1997). These structural models provide constraints on surface gravity as a function of age and temperature, and the two models give consistent results for age, temperature, and gravity. The range of age or gravity for the calculated colors are given at the bottom of the table.

Table 8 shows that the $K-L'$ colors for L dwarfs calculated by Chabrier et al. agree reasonably well with our observations. For T dwarfs their calculated $K-L'$ colors are redder than observed while those of Burrows et al. more closely match our observations. The L' bandpass used here has a bluer cut-on wavelength than that used by either model—compare, for example, the bandpass shown in Figure 1 to that of L'_{AAO} in Figure 9 of Bessell & Brett (1988). Our bandpass will include some of the CH_4 absorption seen in late L and T dwarfs (see also § 5.1). Stephens et al. (2001) show that this difference in bandpass can lead to the model $K-L'$ colors being redder by 0.1 mag for late L dwarfs and by 0.2 mag for mid-T dwarfs; we have confirmed the latter by tests using the observed G1 229B spectrum. The large discrepancy between the observed L' fluxes of T dwarfs and those predicted from the models of Chabrier et al. (1.3 mag at T6) is most likely due to their treatment of dust; the authors acknowledge that dust grains are more likely to exist below, rather than within, the photosphere of T dwarfs, as is assumed by the Burrows et al. models.

The observed $K-M'$ colors of L and T dwarfs are bluer than calculated by either model. The absolute K magnitudes predicted by the models are consistent with our measurements, at least for the small sample of L and T dwarfs with known parallaxes. Thus, if the predicted $K-M'$ colors are too red, then the predicted M -band fluxes are likely to be too large. For T dwarfs, the $K-M'$ discrepancy of ≥ 1.0 mag implies that the models of both Burrows et al. (1997) and Chabrier et al. (2000) predict around three times the observed M -band flux. This is disappointing as model calculations had suggested that the $5 \mu\text{m}$ region would be the preferred wavelength for brown dwarf studies using planned space instruments (Burrows et al. 2001). The discrepancy found here implies that achieving this goal will require higher sensitivity than originally thought.

Differences in the M -filter passbands used for the model calculations and the observations cannot explain the discrepancy. The M' filter used here has half-power wavelengths of $4.57 \mu\text{m}$ and $4.80 \mu\text{m}$ (see Fig. 1). The typical M filter has a half-power bandpass defined by the wavelength range $4.50\text{--}5.00 \mu\text{m}$ (see Fig. 9 of Bessell & Brett 1988). No strong features are expected in the spectra of the A0 calibration star or T dwarfs within these wavelength ranges; for T dwarfs H_2O absorption will be important longward of the M band, and CO absorption is not expected as all the carbon should be in the form of CH_4 (but see the discussion below). F. Allard (2001, private communication), using models similar to those in Chabrier et al., finds no significant difference between $K-M$ and $K-M'$. Calculations we have done with model spectra made available to us by F. Allard and P. Hauschildt, and by D. Saumon and M.

Marley, show the flux through the M and M' filters differs only by 4% at $T_{\text{eff}} = 2000$ K and 9% at $T_{\text{eff}} = 800$ K. Tests using the observed spectrum for the T dwarf Gl 229B imply the effect to be larger but still only 20%.

The models of Burrows et al. (1997) and Chabrier et al. (2000) make very different assumptions about the presence of dust in the photosphere; however, while they calculate very different $K-L'$ colors at $T_{\text{eff}} \approx 1000$ K, their $K-M'$ colors are very similar. Hence it seems that dust does not cause the M' discrepancy observed here. Another possible uncertainty in the models is treatment of molecular opacities. Noll, Geballe, & Marley (1997) and Oppenheimer et al. (1998) have detected CO absorption features in the M -band spectrum of the T6 dwarf Gl 229B. The implied abundance of CO in the photosphere of Gl 229B is much greater than that expected under conditions of thermochemical equilibrium (Fegley & Lodders 1996). This overabundance of CO may be the result of vertical mixing in the atmosphere, a condition not included in the models of Burrows et al. (1997) or Chabrier et al. (2000). Opacity from CO, and/or the change in the temperature-pressure structure of the atmosphere introduced by mixing, may at least partly account for the M -band discrepancy between observations and models. Convolution of the M' filter profile with the Gl 229B spectrum of Noll et al. (1997) shows that the CO absorption bands reduce the M' flux by ~ 0.4 mag; convolution with the wider M filter shows the effect to be ~ 0.7 mag. The latter is close to the observed discrepancy if $T_{\text{eff}} \approx 1300$ K (see Table 8). Further study is clearly warranted.

6. CONCLUSIONS

We present $ZJHKLM'$ photometry for a sample of 58 late-M, L, and T dwarfs, most of which have been classified spectroscopically by G02. A well-defined but relatively new photometric system is used; differences between this and previous near-infrared systems are significant at around the 5% level, but in the case of the T dwarfs the difference at J is $\sim 30\%$ and at L' and M/M' it is $\sim 20\%$. Differences between photometric systems must be taken into account when comparing infrared colors of L and T dwarfs taken from the literature.

We have determined effective temperatures and bolometric corrections where possible, to show that $2200 \gtrsim T_{\text{eff}} \gtrsim 1300$ K for L dwarfs and $1300 \gtrsim T_{\text{eff}} \gtrsim 800$ K for the known T dwarfs. The temperatures derived for late-L dwarfs are consistent with the expected CO to CH₄ transition temperature in brown dwarf atmospheres (Lodders 1999).

We have analyzed the data by examining color-color, color-magnitude, and color-spectral type diagrams. We conclude the following, in order of increasing wavelength:

We find that a filter centered around $1 \mu\text{m}$ (e.g., UKIRT Z) is well suited for measuring the fluxes of brown dwarfs in a region where their energy distributions are rapidly rising. Consequently, the Z filter is useful for flux-calibrating red spectra, as long as the bandpass is accurately known. On the other hand, the pressure-broadened wings of the K I resonance doublet at $0.77 \mu\text{m}$ and the increasing water absorption in the J -band cause $Z-J$ to saturate at ~ 1.8 for L and T dwarfs. Therefore, $Z-J$ is not useful as a discriminator of brown dwarf spectral type.

The onset of CH₄ absorption at the L-T spectral boundary (see G02) causes the $J-H$ and $H-K$ colors of T dwarfs

to become progressively bluer, overlapping the color space occupied by M dwarfs. The $ZJHK$ -band color trends of late-M, L, and T dwarfs show that, although SDSS and 2MASS broadband colors together are superb for identifying *candidate* brown dwarfs, confirmation and classification of all but the later T dwarfs require follow-up spectroscopy or longer baseline photometry.

We find significant scatter in the JHK colors of both L and the later T dwarfs. We suggest that the JHK magnitudes of L dwarfs are sensitive to the presence and composition of dust clouds in their photospheres. We also suggest that the K magnitudes of T dwarfs are sensitive to variations in gravity and/or metallicity that affect the strength of the pressure-induced H₂ opacity in this band. The observed scatter between color and spectral type may imply that there is not a unique relationship between effective temperature and spectral type; more bolometric luminosities are needed to determine whether this is true.

We find that $K-L'$ increases monotonically through most of the M, L, and T classes. A color degeneracy of $K-L' \approx 1.5$ exists between spectral types L6 and T5, most likely due to CH₄ absorption at the blue edge of our L' bandpass, which has been shown by Noll et al. (2000) and Oppenheimer et al. (1998) to be detectable for spectral types around L6 and later. This limits the usefulness of $K-L'$ as an indicator of effective temperature. Of all the color-color combinations spanned by our near-infrared photometry, $J-K$ versus $K-L'$ is the best discriminator of late-M, L, and T spectral types. Except for dwarfs near the L-T boundary, the dwarfs in our sample can be classified photometrically in this color space within one or two subclasses.

We have obtained accurate M' magnitudes for two L dwarfs and two T dwarfs. The M -band fluxes for T dwarfs deduced from our photometry are around three times fainter than predicted by current atmospheric models. This discrepancy may be caused in part by increased opacity due to a higher than expected photospheric abundance of CO, as has been detected by Noll, Geballe, & Marley (1997) and Oppenheimer et al. (1998) for Gl 229B. This discrepancy demonstrates the need for improved models of substellar atmospheres and for more $5 \mu\text{m}$ spectroscopic data, although the results presented here show that such observations will be more difficult than anticipated.

We are very grateful to the staff at UKIRT for their assistance in obtaining the data presented in this paper. Some data were obtained through the UKIRT Service Programme. UKIRT is operated by the Joint Astronomy Centre on behalf of the U. K. Particle Physics and Astronomy Research Council. We are grateful to the referee for helpful comments on the manuscript, to France Allard for calculations of colors through the M' bandpass, to Denise Stephens for prepublication results, and to France Allard, Peter Hauschildt, Didier Saumon, and Mark Marley for making models available for investigating filter bandpass effects. X. F. acknowledges support from NSF grant PHY-0070928 and a Frank and Peggy Taplin Fellowship. G. R. K. is grateful for support to Princeton University and the Humanities Council, and to NASA via grants NAG 5-6734 and NAG 5-8083. D. A. G. acknowledges support from the Center for Astrophysical Studies at Johns Hopkins University. The Sloan Digital Sky Survey (SDSS) is a joint project of The University of Chicago, Fermilab, the Institute for Advanced Study, the Japan Participation Group,

The Johns Hopkins University, the Max-Planck-Institute for Astronomy (MPIA), the Max-Planck-Institute for Astrophysics (MPA), New Mexico State University, Princeton University, the United States Naval Observatory, and the University of Washington. Apache Point Observatory, site of the SDSS telescopes, is operated by the Astrophysical Research Consortium (ARC). Funding for the project has been provided by the Alfred P. Sloan

Foundation, the SDSS member institutions, the National Aeronautics and Space Administration, the National Science Foundation, the US Department of Energy, the Japanese Monbukagakusho, and the Max Planck Society.¹⁶

¹⁶ The SDSS Web site is <http://www.sdss.org>.

REFERENCES

- Ackerman, A. S., & Marley, M. S. 2001, *ApJ*, 556, 872
 Allard, F., Hauschildt, P. H., Alexander, D. R., Tamanai, A., & Schweitzer, A. 2001, *ApJ*, 556, 357
 Bailer-Jones, C. A. L., & Mundt, R. 2001, *A&A*, 367, 218
 Becklin, E. E., & Zuckerman, B. 1988, *Nature*, 336, 656
 Beichman, C. A., Chester, T. J., Skrutskie, M., Low, F. J., & Gillett, F. 1998, *PASP*, 110, 480
 Bessell, M. S., & Brett, J. M. 1988, *PASP*, 100, 1134
 Borysow, A., Jorgensen, U. G., & Zheng, C. 1997, *A&A*, 324, 185
 Burgasser, A. J., et al. 1999, *ApJ*, 522, L65
 Burrows, A., Hubbard, W. B., Lunine, J. I. & Liebert, J. 2001, *Rev. Mod. Phys.*, 73, 719
 Burrows, A., et al. 1997, *ApJ*, 491, 856
 Burrows, A., Marley, M. S., & Sharp, C. M. 2000, *ApJ*, 531, 438
 Chabrier, G., Baraffe, I., Allard, F., & Hauschildt, P. H. 2000, *ApJ*, 542, 464
 Cuby, J. G., Saracco, P., Moorwood, A. F. M., S'Odorico, S., Lidman, C., Comerón, F., & Spyromillo, J. 1999, *A&A*, 349, L41
 Dahn, C., et al. 2000, in *ASP Conf. Ser. 212, Giant Planets to Cool Stars*, ed. C. Griffith & M. Marley (San Francisco: ASP), 79
 Delfosse, X., et al. 1997, *A&A*, 327, L25
 Fan, X., et al. 2000, *AJ*, 119, 928
 Fukugita, M., Ichikawa, T., Gunn, J. E., Doi, M., Shimasaku, K., & Schneider, D. P. 1996, *AJ*, 111, 1748
 Fegley, B., & Lodders, K. 1996, *ApJ*, 472, L37
 Geballe, T. R., Kulkarni, S. R., Woodward, C. E., & Sloan, G. C. 1996, *ApJ*, 467, L101
 Geballe, T. R., Saumon, D., Leggett, S. K., Knapp, G. R., Marley, M. S., & Lodders, K. 2001, *ApJ*, 556, 373
 Geballe, T. R., et al. 2002, *ApJ*, 564, 466 (G02)
 Hawarden, T. G., Leggett, S. K., Letawsky, M. B., Ballantyne, D. R., & Casali, M. M. 2001, *MNRAS*, 325, 563
 Jones, H. R. A., Longmore, A. J., Allard, F., Hauschildt, P. H. 1996, *MNRAS*, 280, 77
 Kirkpatrick, J. D., Allard, F., Bida, T., Zuckerman, B., Becklin, E. E., Chabrier, G., & Baraffe, I. 1999a, *ApJ*, 519, 834
 Kirkpatrick, J. D., Beichman, C. A., & Skrutskie, M. F. 1997, *ApJ*, 476, 311
 Kirkpatrick et al. 1999b, *ApJ*, 519, 802
 Kirkpatrick, J. D., et al. 2000, *AJ*, 120, 447
 Krisciunas, K., Margon, B., & Szkody, P. 1998, *PASP*, 110, 1342
 Leggett, S. K. 1992, *ApJS*, 82, 351
 Leggett, S. K., Allard, F., Geballe, T. R., Hauschildt, P. H., & Schweitzer, A. 2001, *ApJ*, 548, 908
 Leggett, S. K., Allard, F., & Hauschildt, P. H. 1998, *ApJ*, 509, 836
 Leggett, S. K., Allard, F., Dahn, C., Hauschildt, P. H., Kerr, T. H., & Rayner, J. 2000a, *ApJ*, 535, 965
 Leggett, S. K., Toomey, D. W., Geballe, T. R., & Brown, R. H. 1999, *ApJ*, 517, L139
 Leggett, S. K., et al. 2000b, *ApJ*, 536, L35
 Liebert, J., Reid, I. N., Burrows, A., Burgasser, A. J., Kirkpatrick, J. D., & Gizis, J. E. 2000, *ApJ*, 533, L155
 Lodders, K. 1999, *ApJ*, 519, 793
 Martin, E. L., Brandner, W., & Basri, G. 1999a, *Science*, 283, 1718
 Martin, E. L., Delfosse, X., Basri, G., Goldman, B., Forveille, T., & Zapatero Osorio, M. R. 1999b, *AJ*, 118, 2466
 Matthews, K., Nakajima, T., Kulkarni, S. R., & Oppenheimer, B. R. 1996, *AJ*, 112, 1678
 Nakajima, T., Oppenheimer, B. R., Kulkarni, S. R., Golimowski, D. A., Matthews, K., & Durrance, S. T. 1995, *Nature*, 378, 463
 Noll, K. S., Geballe, T. R., Leggett, S. K., & Marley, M. S. 2000, *ApJ*, 541, L75
 Noll, K. S., Geballe, T. R., & Marley, M. S. 1997, *ApJ*, 489, L87
 Oppenheimer, B. R., Kulkarni, S. R., Matthews, K., & van Kerkwijk, M. H. 1998, *ApJ*, 502, 932
 Perryman, M. A. C., et al. 1997, *A&A*, 323, L49
 Reid, I. N., Burgasser, A. J., Cruz, K. L., Kirkpatrick, J. D., & Gizis, J. E. 2001a, *AJ*, 121, 1710
 Reid, I. N., Gizis, J. E., Kirkpatrick, J. D., & Koerner, D. W. 2001b, *AJ*, 121, 489
 Ruiz, M. T., Leggett, S. K., & Allard, F. 1997, *ApJ*, 491, L107
 Saumon, D., Geballe, T. R., Leggett, S. K., Marley, M. S., Freedman, R. S., Lodders, K., Fegley, B., & Sengupta, S. K. 2000, *ApJ*, 541, 374
 Simons, D., & Tokunaga, A. 2001, *PASP*, in press
 Stephens, D. S., Marley, M. S., Noll, K. S., & Chanover, N., 2001, *ApJ*, 556, L97
 Strauss, M. A., et al. 1999, *ApJ*, 522, L61
 Tinney, C. G., Reid, I. N., Gizis, J., & Mould, J. R. 1995, *AJ*, 110, 3014
 Tokunaga, A., & Simons, D. 2001, *PASP*, in press
 Tsuji, T., Ohnaka, K., Aoki, W., & Nakajima, T. 1996, *A&A*, 308, L29
 Tsuji, T., Ohnaka, K., & Aoki, W. 1999, *ApJ*, 520, L119
 Tsvetanov, Z. I., et al. 2000, *ApJ*, 531, L61
 van Altena, W. F., Lee, J. T., & Hoffleit, E. D. 1994, *The General Catalogue of Trigonometric Parallaxes* (New Haven: Yale Univ. Obs.)
 York, D. G., et al. 2000, *AJ*, 120, 1579